S100B drives glioblastoma invasion and migration through TGF-β2-mediated epithelial-mesenchymal transition

XUEMEI LIAO[1,2], YUAN XU[1,3], HONGHONG ZHOU[1,2], QIN YI[1,3], SHIFANG DONG[1,2] and BIN TAN[1,3]

[1]Department of Pediatric Research Institute, Children's Hospital of Chongqing Medical University, National Clinical Research Center for Child Health and Disorders, Ministry of Education Key Laboratory of Child Development and Disorders, Chongqing 400014, P.R. China; [2]Chongqing Key Laboratory of Pediatric Metabolism and Inflammatory Diseases, Chongqing 400014, P.R. China; [3]Key Laboratory of Children's Vital Organ Development and Diseases of Chongqing Health Commission, Chongqing 400014, P.R. China

Received July 16, 2025; Accepted October 27, 2025

DOI: 10.3892/or.2025.9025

Abstract. Glioblastoma (GBM), the most common type of primary malignant brain tumor, is characterized by aggressive cancer cells that contribute to infiltrative growth, thus resulting in therapeutic challenges and a poor prognosis. To explore the molecular mechanisms underlying cell motility and to identify therapeutic targets that may intervene in tumor invasion, public databases were used to investigate the S100B expression profile and the prognosis of patients with tumors. The effects of S100B on a GBM cell line were assessed through lentiviral transduction, as well as cell viability, colony formation, 5-ethynyl-2'-deoxyuridine-based cell proliferation, cross-scratch, and Transwell migration and invasion assays. In addition, a tumor xenograft model was constructed to analyze tumor growth *in vivo*. Reverse transcription-quantitative PCR, western blotting and immunofluorescence staining were utilized to explore the molecular biological mechanisms of the TGF-β2-induced epithelial-mesenchymal transition (EMT) in the S100B-downregulated group. The findings demonstrated that S100B was significantly upregulated in GBM samples and was strongly associated with patient prognosis. *In vitro* and *in vivo* experiments confirmed that downregulation of S100B effectively suppressed the proliferation and tumorigenicity, as well as decreased the invasive and migratory capabilities of LN229 glioblastoma cells. Further investigation revealed that the inhibition of S100B resulted in downregulation of TGF-β2 expression and reversal of the EMT process. Notably, recombinant TGF-β2 restored the cell motility and EMT capacities attenuated by the downregulation of S100B. In conclusion, the present study revealed that S100B may induce the invasion and migration of GBM cells through TGF-β2-induced EMT, providing novel insights and potential therapeutic targets for GBM.

Correspondence to: Dr Bin Tan, Department of Pediatric Research Institute, Children's Hospital of Chongqing Medical University, National Clinical Research Center for Child Health and Disorders, Ministry of Education Key Laboratory of Child Development and Disorders, 2 Zhongshan Road, Yuzhong Chongqing 400014, P.R. China
E-mail: tanbin@hospital.cqmu.edu.cn

Abbreviations: GBM, glioblastoma multiforme; EMT, epithelial-mesenchymal transition; WHO, World Health Organization; DMEM, Dulbecco's Modified Eagle Medium; shS100B, shRNA S100B LN229 GBM cells; NC, negative control LN229 GBM cells; GEPIA, Gene Expression Profiling Interactive Analysis; TCGA, The Cancer Genome Atlas; TISCH, Tumor Immune Single Cell Hub; EdU, 5-ethynyl-2'-deoxyuridine

Key words: S100B, GBM, invasion, migration, EMT, TGF-β2

Introduction

Glioblastoma (GBM) is the most common and deadly type of brain cancer (1). On the basis of the World Health Organization (WHO) guidelines for central nervous system tumor classification, GBM is a grade IV diffuse glioma (2). The GBM cell characteristic of diffuse infiltration has the ability to invade the surrounding normal brain tissue, resulting in recurrence even after complete resection (3). The current standard of care for GBM involves a combination of surgical resection with radiation and chemotherapy (4-6). In recent years, despite advancements in therapeutic efficacy against GBM, its prognosis remains poor. Therefore, it is necessary to elucidate the molecular mechanisms governing the pathogenesis and progression of GBM, while exploring potential therapeutic targets to increase treatment efficacy and prolong patient survival.

S100B, which is located on chromosome 21, is a Ca^{2+}-binding protein of the S100 family, and numerous studies have demonstrated its neurotrophic effects. In the central nervous system, S100B primarily influences the proliferation and differentiation of glial cells, as well as the maintenance of calcium homeostasis (7). Its carboxyl terminus has a strong affinity for Ca^{2+}; when it binds to Ca^{2+}, S100B undergoes conformational changes that expose its target protein-binding site and exerts biological effects through interactions with these target proteins (8,9). Melanoma, ovarian and breast cancer, and other malignant tumors have been observed to express S100B at substantially elevated levels. Furthermore, it is closely associated with tumor development, malignancy and prognosis (10-12). In previous studies, S100B silencing in melanoma cells has been shown to restore p53-mediated apoptosis, which may restrict

malignant cell proliferation (13,14). Moreover, intervention with S100B expression in ovarian cancer stem-like cells has been shown to increase p53 activity and reduce subcutaneous tumor volume, leading to markedly prolonged survival time in nude mice (12). In addition, S100B may drive bevacizumab resistance in ovarian cancer by promoting angiogenesis. Both *in vivo* resistant tumors and *in vitro* S100B-overexpressing cells were found to enhance human umbilical vein endothelial cell migration and tube formation, which can be replicated by exogenous S100B treatment. Mechanistically, endothelial cells uptake tumor-derived S100B, which suppresses FOXO1 and releases β-catenin for nuclear pro-angiogenic signaling (15). Emerging evidence has implicated S100B in GBM pathogenesis, although mechanistic insights remain limited. Serum S100B levels are elevated in patients with glioma compared with those obtained from control individuals with craniocerebral trauma (16). In addition, S100B concentrations are positively associated with tumor grade; they are notably higher in high-grade vs. low-grade glioma, according to the WHO classification system. However, the tissue-specific expression patterns of S100B in GBM, its clinical relevance and its functional roles in tumor progression require further investigation.

The present study identified the upregulated expression of S100B in GBM and its close association with an unfavorable prognosis. By contrast, the inhibition of S100B resulted in suppressed proliferative capacity, and a reduction in invasion, migration and EMT. The results also revealed that downregulation of TGF-β2 was observed upon inhibition of S100B. Consistently, cell invasion, migration and the EMT process were rescued by exogenous recombinant protein TGF-β2 treatment. These findings indicate the role of S100B in promoting GBM progression. The current study elucidates the mechanism by which S100B facilitates GBM cell invasion and migration via the TGF-β2-induced EMT process that exhibits an infiltrative growth pattern, thus providing novel insights for GBM treatment.

Materials and methods

Cell lines and culture. The human GBM cell line LN229 (cat. no. CRL-2611) was obtained from the American Type Culture Collection. The cell line was verified through short tandem repeat testing (Guangzhou Cellcook Biotech Co., Ltd.). The cells were cultured in Dulbecco's modified Eagle's medium (DMEM; cat. no. 11995065; Gibco; Thermo Fisher Scientific, Inc.) supplemented with 10% fetal bovine serum (cat. no. PWL001; Dalian Meilun Biology Technology Co., Ltd.) and 1% penicillin-streptomycin (cat. no. ST488S; Beyotime Institute of Biotechnology) and were incubated at 37˚C with 5% CO_2.

Flow cytometric analysis. A total of $2x10^6$ cells were collected and fixed with 4% paraformaldehyde for 15 min, then washed with PBS. After incubation with S100B antibody (1:200; cat. no. ab52642; Abcam) overnight, the cells were washed with PBS and stained with FITC-Goat Anti-Rabbit IgG secondary antibody (1:200; cat. no. A22120; Abbkine Scientific Co., Ltd.) for 1.5 h. The final wash was completed and used for flow cytometry. Flow cytometric analysis was conducted on a BD FACSCanto™ Flow Cytometer system (10-colour configuration; BD Biosciences), followed by processing of the data using BD FACSDiva Software (BD Biosciences).

Lentiviral transduction to knockdown S100B. LN229 cells were stably transduced with short hairpin (sh)RNA vectors to knockdown S100B. The shRNA vectors were purchased from Shanghai GeneChem Co., Ltd. The S100B shRNA vector (shS100B) sequence was 5'-CTGCCACGAGTTCTTTGAA-3', and the negative control (NC) sequence was 5'-TTCTCCGAA CGTGTCACGT-3'. For transduction of the human GBM cell line LN229, $5x10^4$ cells/well in a 12-well plate were transduced with lentiviral particles (multiplicity of infection, 10) for 12 h. The serum-free medium was then replaced with medium containing 10% FBS. A total of 48 h after lentivirus transduction, the cells were treated with puromycin (cat. no. P8230; Beijing Solarbio Science & Technology Co., Ltd.) working concentration 2.0 μg/ml for 48 h to screen successfully transduced positive cells. At 72 h post-infection, GFP expression was examined using a fluorescence microscope (Nikon Corporation). The validation of shRNA knockdown efficiency of S100B was verified by reverse transcription-quantitative PCR (RT-qPCR), western blot analysis and immunofluorescence (IF) staining. The experimental results were obtained from three replicate experiments using NC LN229 GBM cells as a control for relative quantitative analysis. The IF results were calculated by randomly selecting six fields each time to analyze their mean fluorescence intensity. The ratio of S100B-positive cells to all cells in each field was first calculated separately for the NC and shS100B groups, and then the relative percentage rate of positive cells was calculated using NC as the control group. In addition, the shS100B cells were cultured with recombinant TGF-β2 protein (cat. no. HY-P7119; MedChemExpress) for 48 h to obtain shS100B + TGF-β2 cells, which were used for subsequent experimental analyses.

RT-qPCR. Total RNA was isolated from NC and shS100B LN229 GBM cells using AG RNAex Pro Reagent (cat. no. AG21101; Accurate Biology). RT-qPCR was performed using the ABScript III RT Master Mix for qPCR with gDNA Remover (cat. no. RK20429; ABclonal Biotech Co., Ltd.) and 2X Universal SYBR Green Fast qPCR Mix (cat. no. RK21203; ABclonal Biotech Co., Ltd.) according to the manufacturer's protocol. Thermocycling conditions are included in Tables I and II. GAPDH was used as an internal control and fold change was determined using the relative quantification ($2^{-\Delta\Delta Cq}$) method (16). The sequences of the primers used were as follows: GAPDH forward, 5'-AATGGACAACTGGTCGTG GAC-3' and reverse, 5'-CCCTCCAGGGGATCTGTTTG-3'; S100B forward, 5'-AGCTGGAGAAGGCCATGGTG-3' and reverse, 5'-GAACTCGTGGCAGGCAGTAG-3'; and TGF-β2 forward, 5'-CAGCACACTCGATATGGACCA-3' and reverse, 5'-CCTCGGGCTCAGGATAGTCT-3'.

Western blot analysis. Total protein was extracted from LN229 cells using a Whole Cell Lysis Assay Kit (cat. no. KGB5303-100; Nanjing KeyGen Biotech Co., Ltd.) and a BCA assay (cat. no. KGB2101-500; Nanjing KeyGen Biotech Co., Ltd.) was used to determine the protein concentration. In total, 30 μg equivalent amounts of protein were separated by SDS-PAGE on 15% gels and were transferred to PVDF

Table I. Thermocycling conditions of reverse transcription reaction.

Temperature,˚C	Time, min
37	2
55	15
85	5
4	Hold

Table II. Quantitative PCR reaction conditions.

Step	Temperature,˚C	Time	Number of cycles
Pre-denaturation	95	3 min	1
Cyclic reaction	95	5 sec	40-45
	60	30 sec	

membranes (cat. no. ISEQ00010; MilliporeSigma). The primary antibodies used were anti-S100B (1:200; cat. no. ab52642; Abcam), anti-GAPDH (1:5,000; cat. no. 10494-1-AP; Wuhan Sanying Biotechnology, Inc.) and anti-TGF-β2 (1:200; cat. no. 19999-1-AP; Wuhan Sanying Biotechnology, Inc.). The corresponding secondary antibodies used were horseradish peroxidase (HRP)-conjugated goat anti-rabbit (1:5,000; cat. no. SA00001-2; Wuhan Sanying Biotechnology, Inc.) or HRP-conjugated AffiniPure goat anti-mouse secondary antibodies (1:5,000; cat. no. SA00001-1; Wuhan Sanying Biotechnology, Inc.). After incubation with secondary antibodies, a chemiluminescence system (G:box; Syngene Europe) was used to detect immunoreactive proteins, and the band intensity relative to that of GAPDH was semi-quantified with Quantity One software (version 4.6.2; Bio-Rad Laboratories, Inc.).

In vivo subcutaneous xenograft model. Immunodeficient 4-week-old male nude mice weighing ~15 grams from Chongqing Tengxin Biotechnology Co., Ltd., were used for tumor formation and analysis. Animals were housed in an specific pathogen free (SPF) environment at 23˚C with 30-70% humidity and 12/12-h light/dark cycle. A total of $1x10^6$ NC cells and shS100B cells in 100 μl DMEM were transplanted subcutaneously into the nude mice. Tumor size was measured every 3 days during this period. The tumor size was calculated using the following formula: Volume=width^2 x length/2. A total of six mice were used in the present study. The maximum recorded tumor volume was 122.301 mm^3. At this endpoint, the tumor length and width measured 6.84 and 5.98 mm, respectively. On day 26 post-injection, the nude mice were placed in a designated asphyxiator and CO_2 is passed through it, with the CO_2 displacing about 70% of the gas in the asphyxiator per minute, and the animal is removed after it is completely dead. Death was confirmed by the sustained absence of spontaneous respiration observed for at least two min, followed by the loss of all critical reflexes, including pupillary, corneal, and toe-pinch responses, prior to proceeding with subsequent experiments. Euthanasia of immunodeficient mice was required if tumor growth exceeded 10% of body weight, if individual tumors exceeded 17 mm in diameter, if ulceration, necrosis or infection developed on the surface of the tumor, or if the mouse lost 15% of its body weight. The tumor tissues were immediately fixed with 4% paraformaldehyde for 24 h before being stored in 30% sucrose solution. The fixed and dehydrated tissues were then embedded in O.C.T. compound (cat. no. 4583; Sakura Finetek USA, Inc.), frozen, sectioned, placed on slides and subjected to IF staining.

IF staining. For IF staining, NC and shS100B LN229 GBM cells were fixed with 4% paraformaldehyde, and frozen tissues from NC and shS100B mice were cut into 15-μm sections. Tumor tissues and GBM cells were stained with an anti-S100B antibody (1:200; cat. no. ab52642; Abcam) overnight at 4˚C. After being washed three times with PBS, the samples were incubated with a DyLight 549 goat anti-rabbit IgG (H+L) secondary antibody (1:200; cat. no. A23320; Abbkine Scientific Co., Ltd.) for 1.5 h at 4˚C. The nuclei were stained with 4,6-diamidino-2-phenylindole (cat. no. C1002; Beyotime Institute of Biotechnology) for 15 min. Images were captured using a laser confocal microscope (Nikon A1R; Nikon Corporation) and were prepared via Nikon NIS-Elements AR Analysis 5.20.02.64-bit software for further analysis.

Cell Counting Kit-8 (CCK-8) proliferation analysis. Cell viability was determined using a CCK-8 assay. NC and shS100B LN229 GBM cells were cultured in 96-well plates at 1,000 cells/well. According to the manufacturer's instructions, the cells were incubated with a mixture containing 10 μl CCK solution (cat. no. M4839; Abmole Bioscience, Inc.) and 90 μl culture medium for 2 h at 37˚C. The OD value was acquired at 450 nm using a microplate reader (Epoch; BioTek; Agilent Technologies, Inc.). Notably, OD values were recorded on days 1, 2, 3, 4 and 5.

5-Ethynyl-2'-deoxyuridine (EdU) proliferation analysis. Another method was also used to evaluate the effect of S100B on cell proliferation. Briefly, NC and shS100B LN229 GBM cells were treated with the BeyoClick™ EdU Cell Proliferation Kit with Alexa Fluor 555 (cat. no. C0075L; Beyotime Institute of Biotechnology) according to the manufacturer's instructions. Subsequently, the cells were stained with 4,6-diamidino-2-phenylindole (cat. no. C1002; Beyotime Institute of Biotechnology) for 15 min. Images were captured using a laser confocal microscope (Nikon A1R) and were analyzed with NIS-Elements AR Analysis 5.20.02.64-bit software.

Colony formation assay. NC and shS100B LN229 cells were seeded into 12-well plates at a density of 2,000 cells/well and were cultured at 37˚C and 5% CO_2 for 8 days. On day 4, the medium was replaced with fresh medium. On day 8, the medium was removed, the cells were washed with PBS, and the cells were subsequently fixed with 4% paraformaldehyde for 15 min. Finally, the cells were stained with crystal violet staining solution (cat. no. C0121-100 ml; Beyotime Institute of Biotechnology) for 15 min, and the wells were imaged by

full scanning using a microplate reader (Epoch) to count the number of visible colonies (≥30 cells).

Transwell migration and invasion assays. First, NC and shS100B LN229 cells were cultured in DMEM without FBS for 12 h. Subsequently, $0.5x10^5$ cells were seeded in the upper chambers of Transwell plates (24 wells; 8-μm pore size; cat. no. 353097; Falcon; Corning, Inc.), which were precoated with Matrigel (cat. no. HY-K6002; MedChemExpress) at 37˚C for 30 min for the invasion assay or uncoated for the migration assay. DMEM without FBS was added to the upper chambers, and DMEM with 10% FBS was added to the lower chambers. After 48 h of incubation, the migratory/invasive cells in the lower chambers of the Transwell plate membranes were fixed with 4% paraformaldehyde and stained with crystal violet solution for 15 min. However, the non-migratory/invasive cells in the upper chambers were removed. The number of migratory/invasive cells in the six fields was randomly determined using a microplate reader at x100 magnification. The relative proportion of migrating/invasive cells was calculated using NC as the controls. And the experiment was repeated three times.

Cross-scratch assay. A scratch assay was used to assess the migratory properties of the NC and shS100B groups. Briefly, $1x10^6$ cells were seeded in 6-well plates with complete DMEM, and when the cells formed a confluent monolayer, they were incubated for 24 h at 37˚C in a 5% CO_2 incubator. A cross-scratch was made using a sterile 10-μl pipette tip, and the cells were then washed with sterile PBS to remove nonadherent cells in suspension. The cells were subsequently cultured in DMEM without FBS, and a microplate reader (Epoch) was used to capture the center of the cross-scratch at 0, 24, 48 and 72 h. The areas of the scratches were analyzed using NIS-Elements AR Analysis 5.20.02.64-bit software, and the percentage of migrating cells was calculated. The cell migration rate was calculated as the cell migration area divided by the cross-scratch area.

Database analysis. The Human Protein Atlas (HPA; https://www.proteinatlas.org/) contains both mRNA and protein expression data from different human tissues, and antibodies with different cat. no. have been used to determine the protein expression level. Thus, using this online database, the mRNA and protein expression data of S100B in different types of cancer were obtained. Moreover, the association between gene expression level and survival time was explored via these databases.

The Gene Expression Profiling Interactive Analysis (GEPIA) dataset is an online database used to analyze RNA sequencing data and Genotype-Tissue Expression projects (http://gepia.cancer-pku.cn/). GEPIA can be used to perform analyses including tumor and normal differential expression analysis, patient survival analysis and gene correlation analysis. For the present study, the mRNA expression of S100B in GBM and paired normal tissues was evaluated using this database.

The Cancer Genome Atlas (TCGA; https://www.cancer.gov/ccg/research/genome-sequencing/tcga) is a Cancer Genomics Program, which includes genomic, epigenomic, transcriptomic and proteomic data. Notably, >20,000 primary cancer samples and matched normal samples from 33 cancer types have been molecularly characterized. The database was used to analyze the expression of S100B in different tumor tissues and normal tissues, and its expression in association with patient survival time.

Gene expression profiles of tumor and normal brain samples generated via chips were obtained from the GSE50161 dataset from the Gene Expression Omnibus (https://www.ncbi.nlm.nih.gov/geo/). The online website SangerBOX (http://sangerbox.com/) was used for patient survival analysis.

Single-cell data were sourced from Tumor Immune Single Cell Hub (TISCH; http://tisch.comp-genomics.org/gallery/), which contains single-cell sequencing data from 17 glioma projects. The database was used to access the expression profiles of S100B in different cell types.

Statistical analysis. Statistical analysis was performed using two-tailed unpaired Student's t-test, One-way ANOVA with GraphPad Prism 9.0 software (Dotmatics). All data are presented as the mean ± standard error of the mean. Every experiment was repeated at least three times, and $P<0.05$ was considered to indicate a statistically significant difference.

Results

S100B is highly expressed in GBM tissue. Bioinformatics analyses from two independent databases consistently revealed elevated S100B expression in GBM. The HPA demonstrated significantly higher S100B mRNA levels in GBM, and melanoma compared with other tumor types (Fig. 1A). Notably, this finding was corroborated by TCGA data, where S100B transcription was markedly increased in GBM tissues relative to normal controls, a contrast more pronounced than that detected in other malignancies (Fig. 1B). This phenomenon was subsequently confirmed in the GSE50161 dataset and the GEPIA database (Fig. 1C and D). Immunohistochemical examination demonstrated the distribution and expression pattern of S100B at the protein level in patients with glioma; most samples displayed moderate to strong nuclear and cytoplasmic positivity, which was greater than that of melanoma and other types of cancer (Fig. 1E and F).

High S100B expression is strongly associated with adverse outcomes in glioma. To systematically evaluate the prognostic value of S100B in glioma, multi-omics data from TCGA, GEPIA and SangerBOX databases were analyzed. Survival analysis revealed that patients with elevated S100B expression exhibited significantly shorter overall survival compared with those with lower expression levels (Fig. 2A), indicating its strong association with a poor prognosis. The present study also assessed glioma single-cell transcriptome data from the TISCH database (17), which confirmed that S100B was markedly upregulated in malignant cells (Fig. 2B). This result was further supported by the Synapse (Fig. 2C). These findings strongly implicate S100B as a potential key regulator and a promising molecular target worthy of further mechanistic investigation in glioma therapeutics.

Knockdown of S100B in LN229 cells. Flow cytometric and IF analyses of LN229 GBM cells stained with S100B revealed

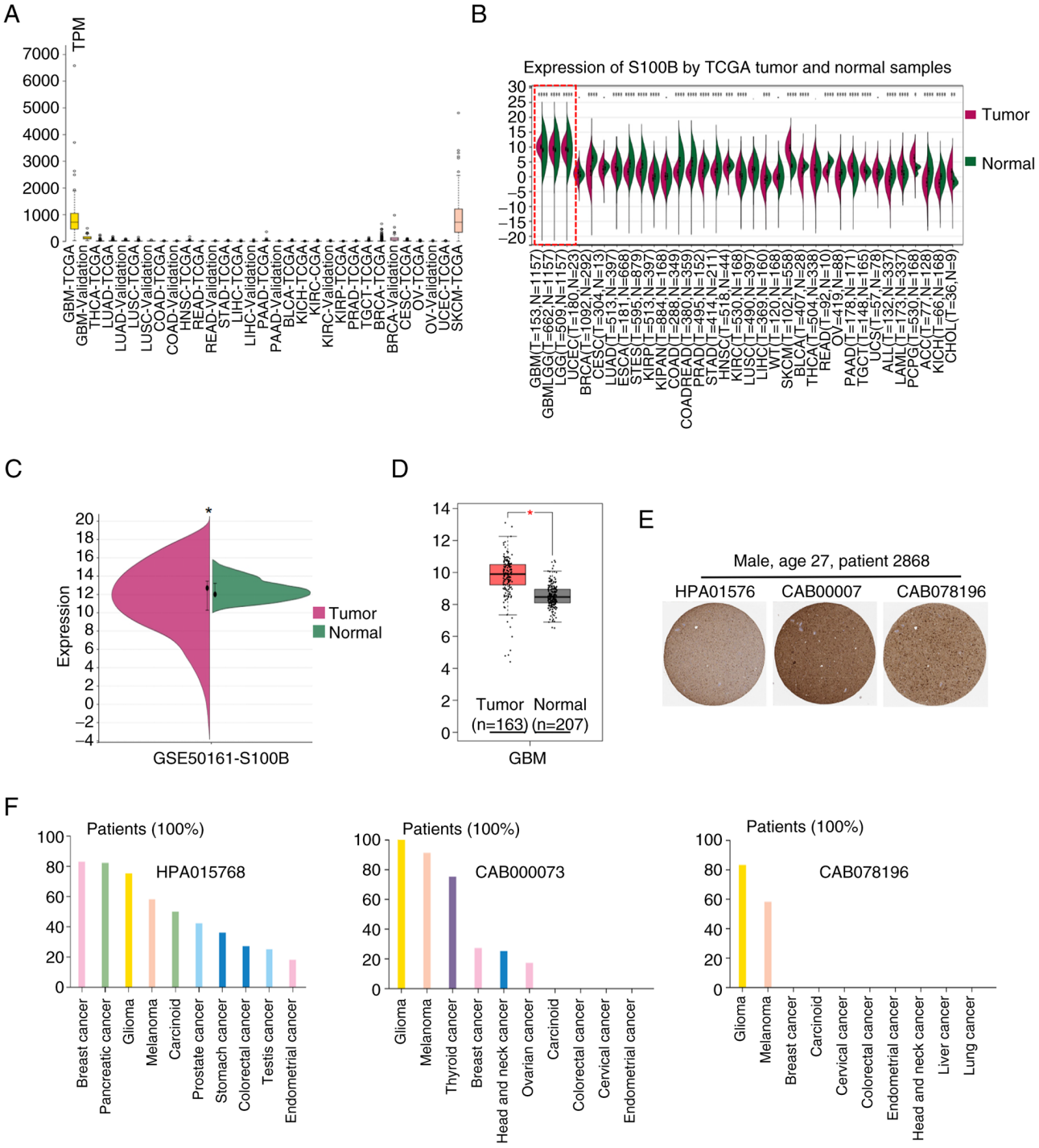

Figure 1. S100B is highly expressed in GBM. (A) mRNA expression of S100B in different tumors was analyzed using the HPA (https://www. proteinatlas.org/). (B) Transcription levels of S100B in 34 types of tumor tissues and their corresponding normal tissues were analyzed by SangerBOX (http://sangerbox.com/). (C and D) GSE50161 dataset and Gene Expression Profiling Interactive Analysis of S100B expression in GBM and normal tissues. (E and F) Immunohistochemical staining of different tumor samples and representative images in glioma with three different S100B antibodies; these data were obtained from the HPA. *P<0.05, **P<0.01, ***P<0.001 and ****P<0.0001. GBM, glioblastoma multiforme; HPA, Human Protein Atlas; TCGA, The Cancer Genome Atlas.

that the percentage of positive cells was as high as 99.9% (Fig. 3A and B). These results confirmed that S100B is highly expressed in the GBM cell line LN229. Lentiviral transduction with shS100B induced intracellular S100B suppression at both transcriptional and translational levels, as indicated by significantly reduced mRNA expression and diminished protein abundance compared with that in the NC group (Fig. 3C-E). Concurrent IF analysis confirmed this knockdown efficiency at the cellular level, with both mean intensity and S100B-positive cells decreased in the shS100B-treated group (Fig. 3F). According to the aforementioned findings, a stable cell line with low S100B expression was successfully constructed.

Target-oriented S100B suppresses LN229 proliferative capacity in vitro and tumorigenicity in vivo. Colony formation assays demonstrated that S100B knockdown

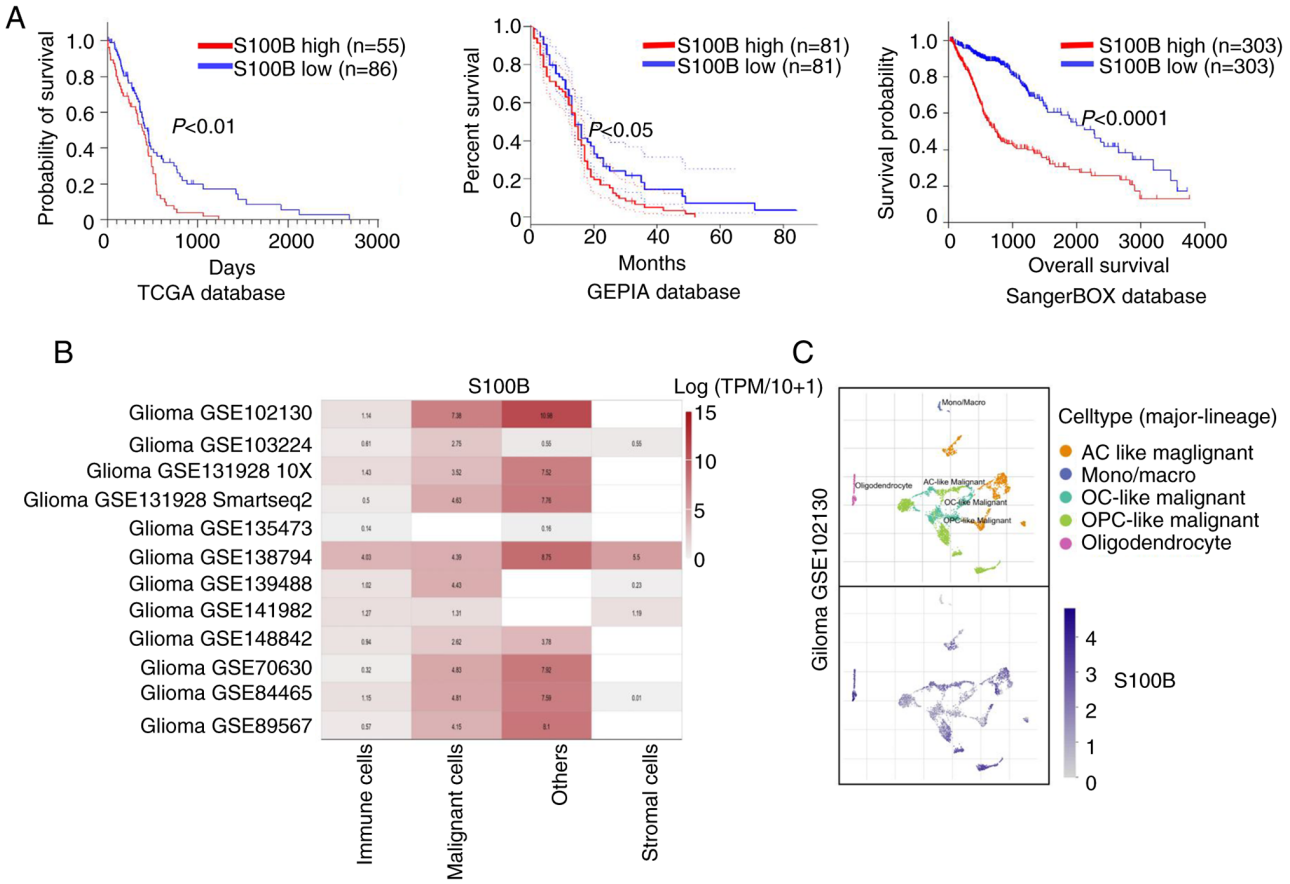

Figure 2. High expression of S100B is associated with a poor prognosis. (A) Survival curve analysis of the prognostic significance of the high and low mRNA expression levels of S100B in glioma based on TGCA, Gene Expression Profiling Interactive Analysis and SangerBOX databases. (B) Single-cell sequencing data from TISCH analyzing the average expression of S100B in different cell types across datasets. (C) Expression distribution and relative expression levels of S100B in different cell types in glioma tissue. TCGA, The Cancer Genome Atlas.

significantly impaired clonogenic potential (Fig. 4A), a finding corroborated by EdU incorporation assays showing significantly decreased DNA synthesis in shS100B LN229 cells (Fig. 4B). Furthermore, the results of the CCK-8 assay confirmed that the inhibition of S100B strongly suppressed the proliferation of LN229 cells (Fig. 4C). To evaluate the effects of S100B on tumorigenicity, NC and shS100B cells were transplanted into nude mice. Quantitative analysis revealed that xenograft tumors in the shS100B group exhibited significantly slower growth kinetics compared with those in the NC group (Fig. 4D). Consistently, endpoint measurements demonstrated a statistically significant reduction in tumor volume within the shS100B cohort relative to the NC group (Fig. 4E). Upon termination of the experiment at day 26 post-implantation, histopathological examination of resected tumors showed well-circumscribed masses without evidence of local tissue invasion or metastatic dissemination. This observation indicated that the subcutaneous xenograft model, while suitable for evaluating primary tumor growth parameters, has limitations in assessing invasive and migratory phenotypes. Subsequently, IF staining of frozen sections demonstrated that S100B expression in shS100B LN229 tumor tissue was significantly lower than that in the NC group (Fig. 4F). These collective findings strongly suggest that S100B depletion attenuates tumorigenic capacity in this preclinical model.

Cell invasion and migration are decreased in the S100B-knockdown group via the inhibition of EMT. The current study further examined the effects of S100B on GBM cell invasion and migration. Wound healing assays revealed a significantly reduced migratory capability in the shS100B group compared with that in the NC group (Fig. 5A). Furthermore, Transwell assays with or without Matrigel coating demonstrated significantly fewer invasive/migratory cells in the shS100B group vs. the NC group (Fig. 5B and C). Collectively, these results demonstrated that S100B knockdown could attenuate the invasive and migratory capacities of GBM cells. To elucidate the molecular mechanism by which S100B affects the invasion and migration of GBM cells, transcriptome sequencing of NC and shS100B LN229 cells was performed. RNA sequencing identified 2,294 differentially expressed genes (fold change >2, P<0.05), comprising 1,130 upregulated and 1,164 downregulated genes between the two groups (Fig. 5D). Gene Ontology (GO) analyses revealed that the induction of mesenchyme morphogenesis, a biological process related to EMT, was among the 20 pathways with the greatest differences in downregulated genes (Fig. 5E). The expression levels of the EMT markers E-cadherin, N-cadherin and vimentin were subsequently analyzed in both the NC and shS100B groups. S100B downregulation upregulated E-cadherin, whereas it downregulated N-cadherin and vimentin, suggesting suppression of EMT, which could

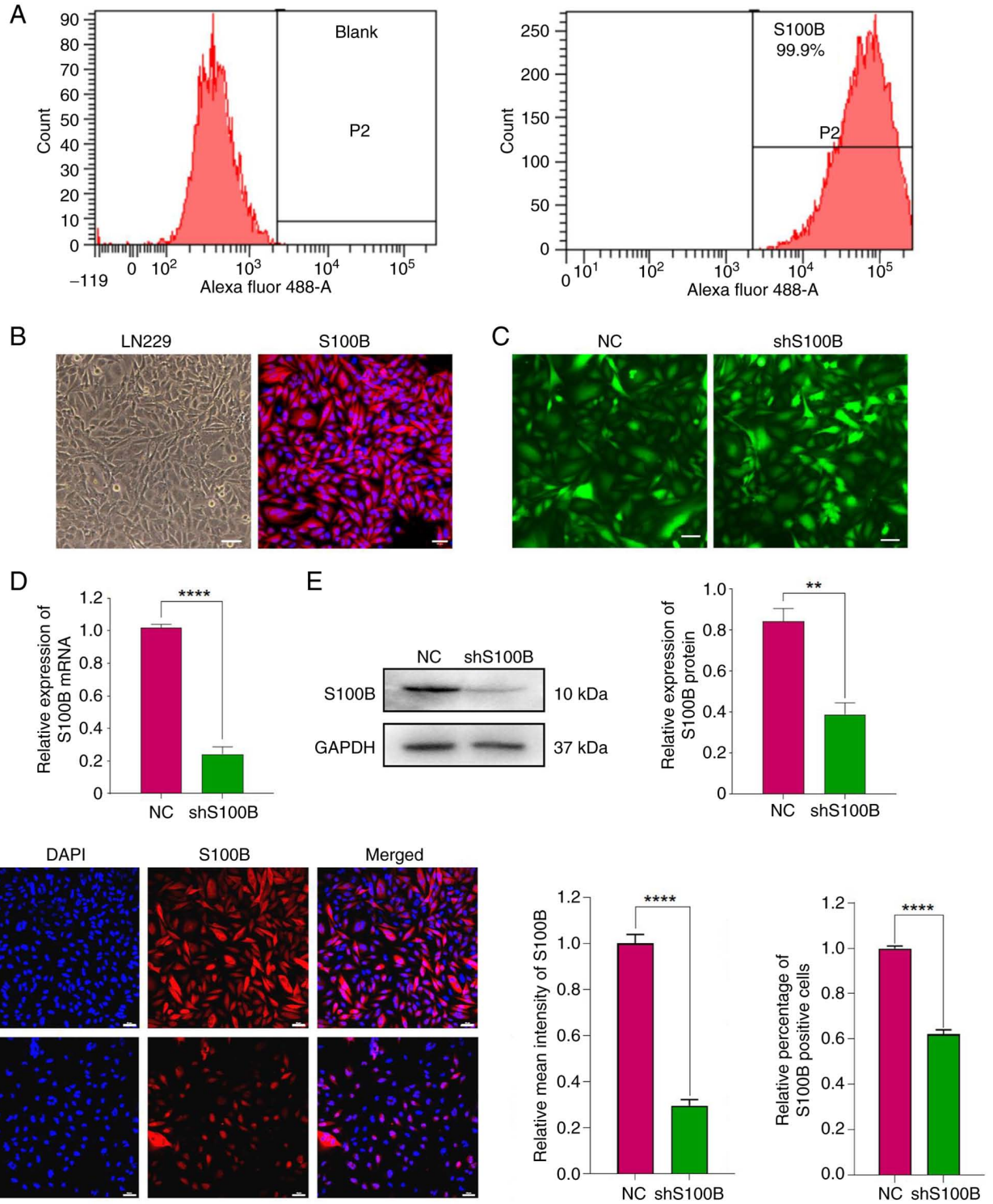

Figure 3. Lentiviral transduction-induced knockdown of S100B in the LN229 glioblastoma multiforme cell line. (A) Detection of S100B expression in LN229 cells by flow cytometry. (B) Representative immunofluorescence images of S100B. Scale bars, 50 μm. (C) LN229 glioma cells were transduced with shS100B and negative control vectors. (D and E) mRNA and protein levels of S100B were analyzed by reverse transcription-quantitative PCR and western blotting. Data are presented as the mean ± SEM. (F) S100B expression in NC and shS100B groups was measured by immunofluorescence staining. DAPI represents cell nuclei. Scale bar, 50 μm. The statistical analyses of the relative mean fluorescence intensity and the relative percentage of positive cells were conducted. Data are presented as the mean ± SEM. **P<0.01 and ****P<0.0001. shS100B, shRNA S100B; NC, negative control.

consequently impair the invasive and migratory capacities of GBM cells (Fig. 5F).

S100B affects the EMT process through TGF-β2. During mesenchyme morphogenesis pathway activation, the EMT-associated gene TGF-β2 exhibited significant downregulation (Fig. 6A). This suppression was further validated by RT-qPCR and western blotting in S100B-knockdown cells (Fig. 6B and C). Accordingly, it was hypothesized that S100B may influence GBM cell motility through TGF-β2-mediated EMT. To confirm this hypothesis, GBM cells with downregulated S100B expression were treated with human recombinant TGF-β2

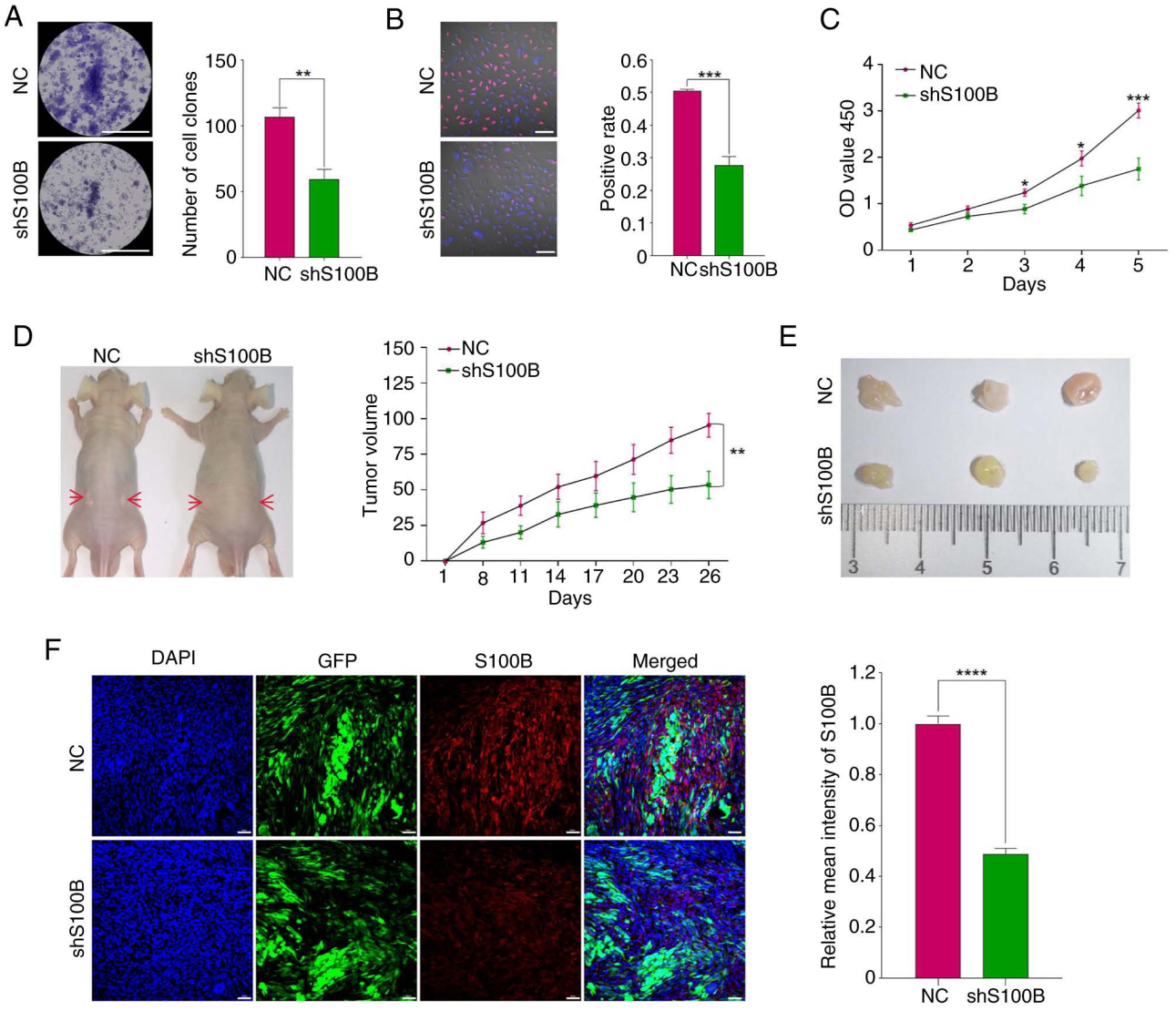

Figure 4. S100B affects the proliferation of LN229 cells and tumor growth *in vivo*. (A) Colony formation assay assessed the proliferative capacity of NC and shS100B groups, Scale bar, 500 μm. (B) DNA synthesis ability was assessed using the EdU assays. Scale bar, 50 μm. (C) Cell Counting Kit-8 assay of proliferation in NC and shS100B LN229 glioblastoma multiforme cells. (D and E) Subcutaneous tumor model, tumor size and volume. (F) Representative immunofluorescence staining images of S100B in tumor tissue sections. DAPI represents cell nuclei. Statistical analysis of relative mean fluorescence intensity of S100B was performed. Data are presented as the mean ± SEM. Scale bar, 100 μm. *P<0.05, **P<0.01, ***P<0.001 and ****P<0.0001. shS100B, shRNA S100B; NC, negative control.

protein. The experimental results revealed that compared with those in the shS100B group, the shS100B + TGF-β2 group had stronger migratory and invasive properties (Fig. 6D and E). Furthermore, E-cadherin was reduced, whereas N-cadherin and vimentin were notably restored in the shS100B + TGF-β2 group (Fig. 6F). These results indicated that downregulation of S100B may attenuate TGF-β2-induced EMT, as well as cell invasion and migration.

Discussion

GBM is the most aggressive and common type of malignant brain tumor in the central nervous system. Patients with GBM have an overall median survival time of 12-16 months (18,19), and a 5-year survival rate of <5% (20,21). GBM possesses highly aggressive tumor cells that proliferate in an infiltrative manner, which results in the absence of a clear boundary between tumor and healthy areas of brain tissue, making it difficult to completely remove the tumor during surgery. Although treatment efficacy has improved with the use of temozolomide and other combination therapies, the prognosis for patients with GBM has remained unfavorable for the past 20 years (22). Therefore, identifying the cellular mechanisms of GBM invasion and preventing its infiltrative growth by means of molecularly specific therapeutic approaches may be valuable in enhancing treatment effectiveness and extending patient survival.

Currently, there are limited findings on the molecular signaling pathway that underlies the effects of S100B on the migration and invasion of GBM, and there is little research on the association between S100B and glioma, especially GBM. S100B is a member of the multigene family of Ca^{2+}-binding proteins with EF-hand motifs, which regulate cellular activities such as metabolism, motility and proliferation. Notably,

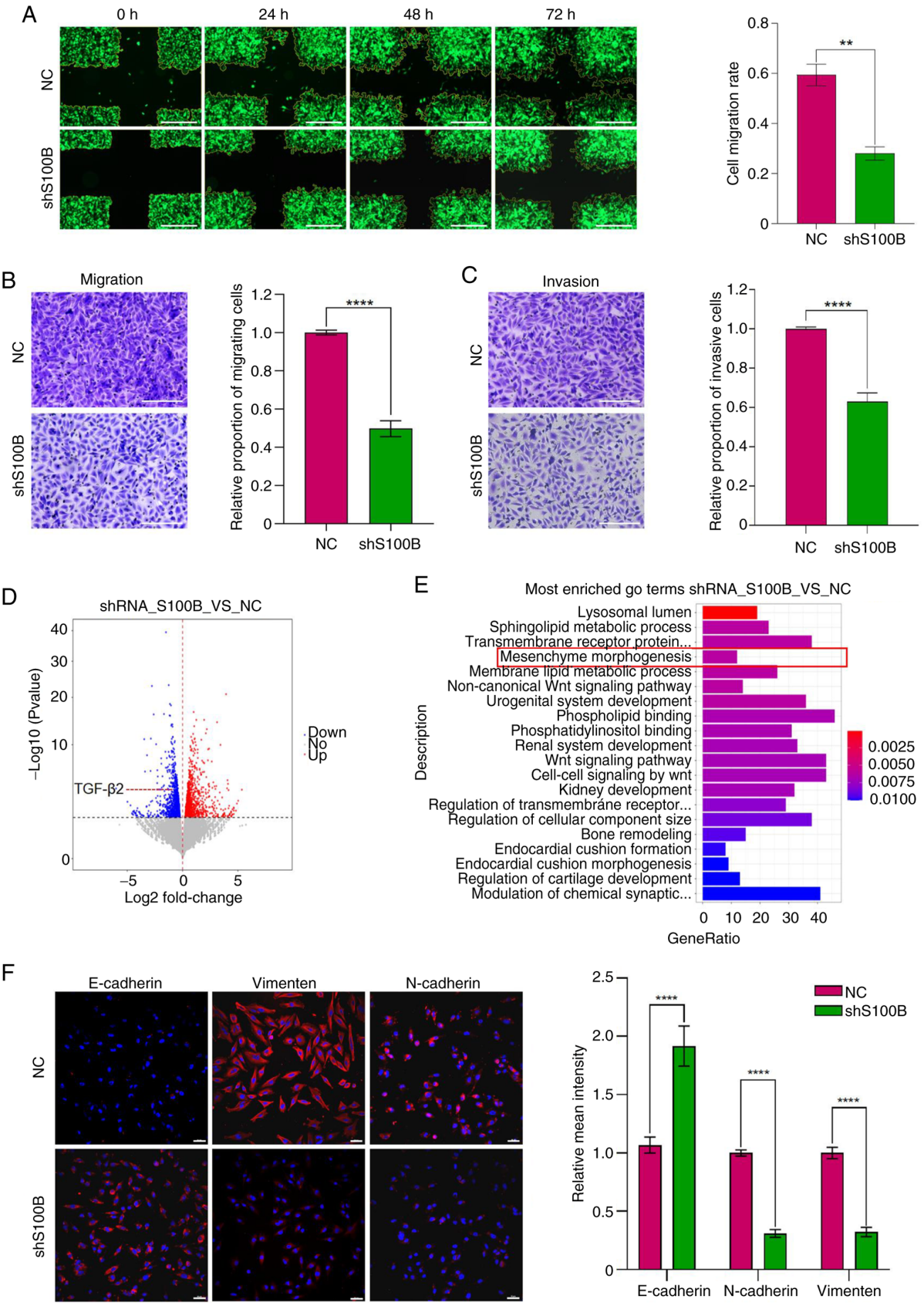

Figure 5. S100B affects the invasion and migration of GBM cells via epithelial-mesenchymal transition. (A) Detection of cell migration ability by cross-scratch assay; Scale bar, 500 μm. Cell migration rate = Cell migration area/cross scratch area. (B and C) Transwell assays analyzed the migratory and invasive capacity of NC and shS100B GBM cells, Scale bar, 200 μm. Relative proportion of migratory or invasive cells: Number of migratory or invasive cells in shS100B group/number of migratory or invasive cells in NC group. (D) Volcano plot showing the DEGs in the NC and shS100B groups. (E) GO enrichment analysis of the functions of downregulated DEG. (F) E-cadherin, N-cadherin and vimentin expression in NC and shS100B LN229 cells were measured by immunofluorescence staining. Blue represents cell nuclei, red represents E-cadherin, N-cadherin and vimentin. Statistical analysis of relative mean fluorescence intensity was performed. Scale bar, 50 μm. Data are presented as the mean ± SEM. **P<0.01 and ****P<0.0001. GBM, glioblastoma multiforme; shS100B, shRNA S100B; NC, negative control; DEGs, differentially expressed genes; GO, Gene Ontology.

A

ID	Description	pvalue	p.adjust	qvalue	Gene name
GO:0072132	mesenchyme morphogenesis	0.00000504	0.006105	0.00558806	**TGFβ2**/WNT5A/SNAI2/HEY1/MYC/TGFBR1/DCHS1/BMPR1A/ACTA2/TMEM100/TBX2/SNAI1

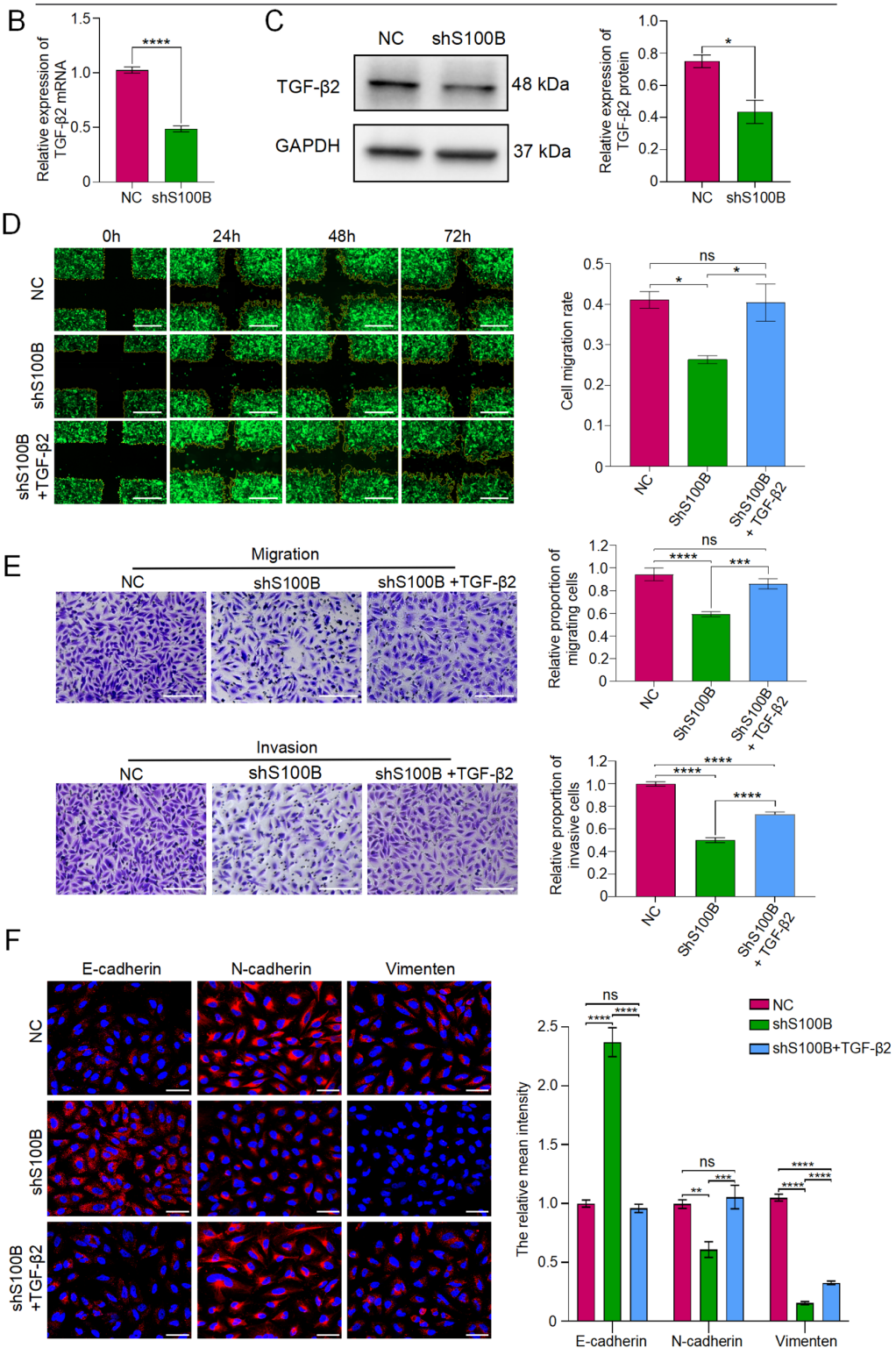

Figure 6. TGF-β2 induces epithelial-mesenchymal transition and enhances the invasion and migration of glioblastoma multiforme cells. (A) Relevant down-regulated genes of the mesenchyme morphogenesis pathway. (B and C) Expression of TGF-β2 in NC and shS100B LN229 cells was analyzed by reverse transcription-quantitative PCR and western blotting. (D) Cross-scratch assay evaluated the migratory capacity of NC, shS100B and shS100B + TGF-β2 groups, Scale bar, 500 μm. (E) Transwell assay analyzed the migratory or invasive capacity of NC, shS100B and shS100B + TGF-β2 groups; Scale bar, 200 μm. Relative proportion of migratory or invasive cells: Number of migratory or invasive cells in shS100B group or shS100B + TGF-β2 group/number of migrated or invaded cells in NC group. (F) E-cadherin, N-cadherin and vimentin were analyzed by immunofluorescence staining. Blue represents cell nuclei, and red represents E-cadherin, N-cadherin and vimentin. Scale bar, 50 μm. Data are presented as the mean ± SEM. *P<0.05, **P<0.01, ***P<0.001 and ****P<0.0001. NC, negative control; shS100B, shRNA S100B.

there is clear evidence that S100B is elevated in primary malignant melanoma (13,14). The results of the present study reported a significantly elevated expression of S100B in both GBM and melanoma samples, as revealed using the HPA database analysis. Our previous studies have indicated that S100B is highly expressed in mouse C6 (23), and in human U251 and LN229 cell lines. In other databases, S100B was shown to be negatively associated with patient survival time, and higher S100B expression was indicated to result in higher mortality in patients with GBM. In a previous *in vitro* study, S100B was shown to promote the proliferation of U251 and T98G GBM cells (24). Furthermore, overexpression of S100B has been reported to upregulate CCL2 secretion in G261 glioma cells, leading to increased infiltration of tumor-associated macrophages into the tumor, increased secretion of inflammatory factors and tumor angiogenesis, which is favorable to enhance the growth of malignant tumors (25). By contrast, decreasing S100B expression in a murine glioma model has been reported to alter the tumor microenvironment (TME), inhibit tumor-associated macrophage migration and suppress tumor progression (26).

The current study demonstrated that targeted knockdown of S100B using shRNA significantly inhibited GBM progression both *in vitro* and *in vivo*, establishing S100B as a critical regulator of GBM pathogenesis and a potential prognostic biomarker. Notably, S100B silencing in LN229 cells significantly reduced cellular invasion and migration *in vitro*, suggesting its pivotal role in tumor metastasis. However, the precise molecular mechanisms underlying these effects remain to be elucidated through further investigation. GO pathway analysis revealed that multiple pathways, including mesenchyme morphogenesis, were enriched. Despite the fact that neural tissue does not originate from a traditional epithelial setting, there is now substantial evidence that the process known as EMT drives glioma invasion and migration in the brain (27,28). Cancer cells undergo EMT, allowing them to acquire mesenchymal characteristics that facilitate invasion and migration. Throughout this process, cancer cells lose intercellular adhesion and epithelial cell polarity, which is accompanied by a downregulation of E-cadherin, ultimately resulting in decreased cell-to-cell or cell-to-extracellular matrix adhesion. Moreover, N-cadherin and vimentin expression is upregulated (29). The current investigation revealed that the process of EMT was reversed following the knockdown of S100B and resulted in inhibition of tumor cell invasion and migration, thus indicating that S100B serves an important role in regulating EMT. The results of the present study highlighted that TGF-β2 may be a vital signaling molecule that is associated with mesenchyme morphogenesis and management of the EMT process in GBM. TGF-β2 is a member of the TGF-β family, which also includes TGF-β1 and TGF-β3. These three subtypes of TGF-β (TGF-β1-3) have the ability to induce EMT in epithelial cells (30-33). By contrast, inhibition or deletion of TGF-β expression can trigger dysregulation of EMT function (34-36). According to the RNA sequencing results of the present study, suppression of S100B resulted in significant downregulation of TGF-β2, but not of TGF-β1 or TGF-β3.

In the present study, the addition of exogenous recombinant TGF-β2 protein restored the EMT phenotype, which was inhibited by S100B knockdown, and restored the invasiveness and migratory ability of the LN229 cell line. It has been demonstrated that TGF-β mediates the EMT of various tumors, including GBM. For example, it has been documented that TGF-β causes GBM cells to pass through a mesenchymal phenotypic transition via enhancing the expression of ZEB and pSmad2 (37). Enhydrin hinders EMT, thereby minimizing both migration and invasion of GBM cells, by mediating the Jun/Smad7/TGF-β1 signaling process (38). Acidosis adaptation in cervical and colorectal cancer cells has been shown to lead to autocrine secretion of TGF-β2, which stimulates the formation of lipid droplets and facilitates the EMT of tumor cells to support malignant progression, such as invasion (39). In gastric cancer, HOXA10 mediates EMT to promote metastasis by regulating the TGF-β2/Smad/METTL3 signaling axis (40). The present findings suggest a close association between TGF-β2, and tumor migration and invasion in GBM. However, to the best of the authors' knowledge, there are no studies at present on the potential role of the S100B-TGFβ2 axis in promoting GBM cell invasiveness and migratory ability through the EMT.

The present study revealed that S100B was predominantly upregulated in GBM tissue, and its elevated expression levels were associated with shorter patient survival time, indicating an adverse prognostic impact. Inhibition of S100B resulted in attenuated cell proliferation, invasion, migration and EMT. Moreover, S100B knockdown induced downregulation of TGF-β2 expression, and decreased cell invasion and migration, whereas the EMT process was restored by the addition of recombinant TGF-β2 protein. From the perspective of EMT, the current study elucidated the mechanism by which S100B promotes the motility of glioma cells and also revealed that S100B modulates the expression of TGF-β2 to mediate the occurrence of EMT. These valuable findings indicate that S100B may be an important marker and potential target site for GBM therapies. Despite elucidating the pivotal role of S100B in promoting GBM cell migration and invasion through modulation of the TGF-β2/EMT axis *in vitro*, the current study is inherently limited by the absence of *in situ* validation, a critical gap given the profound influence of the complex EMT on metastatic behavior. To further investigate the role of S100B in GBM progression, the intracranial GBM xenograft model in immunocompromised mice is recommended to enable rigorous assessment of the impact of S100B on invasion via bioluminescence and histopathological analyses. Furthermore, the transparent zebrafish system with GFP-labeled tumor cells may offer real-time visualization of micro-metastasis formation (41,42). This dual-model approach would not only complement the present *in vitro* findings but also provide mechanistic insights into the role of S100B across different biological contexts. Future investigations will leverage these platforms to evaluate the therapeutic potential of S100B through targeted genetic interventions, potentially paving the way for novel anti-metastatic strategies in GBM.

Acknowledgements

Not applicable.

Funding

The present study was supported by the Youth Basic Research Project from the Ministry of Education Key Laboratory of Child Development and Disorders (grant no. YBRP-202113) and the Science and Technology Research Program of the Chongqing Municipal Education Commission (grant no. KJQN202400427).

Availability of data and materials

The data generated in the present study may be requested from the corresponding author.

Authors' contributions

XL obtained most of the study's outcome data independently, analyzed and interpreted the data, drafted the manuscript, and obtained funding. YX made significant contributions to the acquisition and analysis of part of the data, and provided valuable assistance in conducting a portion of the experiments. HZ, QY and SD were involved in obtaining some of the research results. BT presented the original research concept and design, analyzed and interpreted the data, revised the contents of the manuscript, obtained funding and supervised the research. All authors read and approved the final version of the manuscript. XL and BT confirm the authenticity of all the raw data.

Ethics approval and consent to participate

The animal use protocol was reviewed and approved by the Ethics Committee of Children's Hospital of Chongqing Medical University (IACUC approval no: CHCMU-IACUC20210114024; Chongqing, China).

Patient consent for publication

Not applicable.

Competing interests

The authors declare that they have no competing interests.

References

1. Tan AC, Ashley DM, López GY, Malinzak M, Friedman HS and Khasraw M: Management of glioblastoma: State of the art and future directions. CA Cancer J Clin 70: 299-312, 2020.
2. Louis DN, Perry A, Wesseling P, Brat DJ, Cree IA, Figarella-Branger D, Hawkins C, Ng HK, Pfister SM, Reifenberger G, *et al*: The 2021 WHO classification of tumors of the central nervous system: A summary. Neuro Oncol 23: 1231-1251, 2021.
3. Sahm F, Capper D, Jeibmann A, Habel A, Paulus W, Troost D and von Deimling A: Addressing diffuse glioma as a systemic brain disease with single-cell analysis. Arch Neurol 69: 523-526, 2012.
4. Omuro A and DeAngelis LM: Glioblastoma and other malignant gliomas: A clinical review. JAMA 310: 1842-1850, 2013.
5. Alexander BM and Cloughesy TF: Adult glioblastoma. J Clin Oncol 35: 2402-2409, 2017.
6. McKinnon C, Nandhabalan M, Murray SA and Plaha P: Glioblastoma: Clinical presentation, diagnosis, and management. BMJ 374: n1560, 2021.
7. Donato R, Cannon BR, Sorci G, Riuzzi F, Hsu K, Weber DJ and Geczy CL: Functions of S100 proteins. Curr Mol Med 13: 24-57, 2013.
8. Schafer BW and Heizmann CW: The S100 family of EF-hand calcium-binding proteins: Functions and pathology. Trends Biochem Sci 21: 134-140, 1996.
9. Donato R, Sorci G, Riuzzi F, Arcuri C, Bianchi R, Brozzi F, Tubaro C and Giambanco I: S100B's double life: intracellular regulator and extracellular signal. Biochim Biophys Acta 1793: 1008-1022, 2009.
10. Xiong TF, Pan FQ and Li D: Expression and clinical significance of S100 family genes in patients with melanoma. Melanoma Res 29: 23-29, 2019.
11. Yen MC, Huang YC, Kan JY, Kuo PL, Hou MF and Hsu YL: S100B expression in breast cancer as a predictive marker for cancer metastasis. Int J Oncol 52: 433-440, 2018.
12. Yang T, Cheng J, Yang Y, Qi W, Zhao Y, Long H, Xie R and Zhu B: S100B mediates stemness of ovarian cancer stem-like cells through inhibiting p53. Stem Cells 35: 325-336, 2017.
13. Lin J, Yang Q, Yan Z, Markowitz J, Wilder PT, Carrier F and Weber DJ: Inhibiting S100B restores p53 levels in primary malignant melanoma cancer cells. J Biol Chem 279: 34071-34077, 2004.
14. Roy Choudhury S, Heflin B, Taylor E, Koss B, Avaritt NL and Tackett AJ: CRISPR/dCas9-KRAB-mediated suppression of S100b restores p53-mediated apoptosis in melanoma cells. Cells 12: 730, 2023.
15. Xu H, Li W, Yue H, Bai Y, Li J, Lu X and Wang J: S100B induces angiogenesis via the clathrin/FOXO1/β-catenin signaling pathway and contributes to bevacizumab resistance in epithelial ovarian cancer. J Adv Res: May 31, 2025 (Epub ahead of print).
16. Livak KJ and Schmittgen TD: Analysis of relative gene expression data using real-time quantitative PCR and the 2(-Delta Delta C(T)) method. Methods 25: 402-408, 2001.
17. Sun D, Wang J, Han Y, Dong X, Ge J, Zheng R, Shi X, Wang B, Li Z, Ren P, *et al*: TISCH: A comprehensive web resource enabling interactive single-cell transcriptome visualization of tumor microenvironment. Nucleic Acids Res 49 (D1): D1420-D1430, 2021.
18. Stupp R, Mason WP, van den Bent MJ, Weller M, Fisher B, Taphoorn MJ, Belanger K, Brandes AA, Marosi C, Bogdahn U, *et al*: Radiotherapy plus concomitant and adjuvant temozolomide for glioblastoma. N Engl J Med 352: 987-996, 2005.
19. Wen PY and Kesari S: Malignant gliomas in adults. N Engl J Med 359: 492-507, 2008.
20. Stupp R, Hegi ME, Mason WP, van den Bent MJ, Taphoorn MJ, Janzer RC, Ludwin SK, Allgeier A, Fisher B, Belanger K, *et al*: Effects of radiotherapy with concomitant and adjuvant temozolomide versus radiotherapy alone on survival in glioblastoma in a randomised phase III study: 5-year analysis of the EORTC-NCIC trial. Lancet Oncol 10: 459-466, 2009.
21. Ostrom QT, Gittleman H, de Blank PM, Finlay JL, Gurney JG, McKean-Cowdin R, Stearns DS, Wolff JE, Liu M, Wolinsky Y, *et al*: American brain tumor association adolescent and young adult primary brain and central nervous system tumors diagnosed in the United States in 2008-2012. Neuro Oncol 18 (Suppl 1): i1-i50, 2016.
22. Witthayanuwat S, Pesee M, Supaadirek C, Supakalin N, Thamronganantasakul K and Krusun S: Survival analysis of glioblastoma multiforme. Asian Pac J Cancer Prev 19: 2613-2617, 2018.
23. Tan B, Shen L, Yang K, Huang D, Li X, Li Y, Zhao L, Chen J, Yi Q, Xu H, *et al*: C6 glioma-conditioned medium induces malignant transformation of mesenchymal stem cells: Possible role of S100B/RAGE pathway. Biochem Biophys Res Commun 495: 78-85, 2018.
24. Hu Y, Song J, Wang Z, Kan J, Ge Y, Wang D, Zhang R, Zhang W and Liu Y: A novel S100 family-based signature associated with prognosis and immune microenvironment in glioma. J Oncol 2021: 3586589, 2021.
25. Wang H, Zhang L, Zhang IY, Chen X, Da Fonseca A, Wu S, Ren H, Badie S, Sadeghi S, Ouyang M, *et al*: S100B promotes glioma growth through chemoattraction of myeloid-derived macrophages. Clin Cancer Res 19: 3764-3775, 2013.
26. Gao H, Zhang IY, Zhang L, Song Y, Liu S, Ren H, Liu H, Zhou H, Su Y, Yang Y and Badie B: S100B suppression alters polarization of infiltrating myeloid-derived cells in gliomas and inhibits tumor growth. Cancer Lett 439: 91-100, 2018.

27. Kahlert UD, Joseph JV and Kruyt FAE: EMT- and MET-related processes in nonepithelial tumors: Importance for disease progression, prognosis, and therapeutic opportunities. Mol Oncol 11: 860-877, 2017.
28. Xie C, Zhou M, Lin J, Wu Z, Ding S, Luo J, Zhan Z, Cai Y, Xue S and Song Y: EEF1D promotes glioma proliferation, migration, and invasion through EMT and PI3K/Akt pathway. Biomed Res Int 2020: 7804706, 2020.
29. Dongre A and Weinberg RA: New insights into the mechanisms of epithelial-mesenchymal transition and implications for cancer. Nat Rev Mol Cell Biol 20: 69-84, 2019.
30. Miettinen PJ, Ebner R, Lopez AR and Derynck R: TGF-beta induced transdifferentiation of mammary epithelial cells to mesenchymal cells: Involvement of type I receptors. J Cell Biol 127: 2021-2036, 1994.
31. Piek E, Moustakas A, Kurisaki A, Heldin CH and ten Dijke P: TGF-(beta) type I receptor/ALK-5 and Smad proteins mediate epithelial to mesenchymal transdifferentiation in NMuMG breast epithelial cells. J Cell Sci 112: 4557-4568, 1999.
32. Valcourt U, Kowanetz M, Niimi H, Heldin CH and Moustakas A: TGF-beta and the Smad signaling pathway support transcriptomic reprogramming during epithelial-mesenchymal cell transition. Mol Biol Cell 16: 1987-2002, 2005.
33. Gao J, Zhu Y, Nilsson M and Sundfeldt K: TGF-β isoforms induce EMT independent migration of ovarian cancer cells. Cancer Cell Int 14: 72, 2014.
34. Su J, Morgani SM, David CJ, Wang Q, Er EE, Huang YH, Basnet H, Zou Y, Shu W, Soni RK, *et al*: TGF-beta orchestrates fibrogenic and developmental EMTs via the RAS effector RREB1. Nature 577: 566-571, 2020.
35. Xu J, Lamouille S and Derynck R: TGF-beta-induced epithelial to mesenchymal transition. Cell Res 19: 156-172, 2009.
36. Leung DHL, Phon BWS, Sivalingam M, Radhakrishnan AK and Kamarudin MNA: Regulation of EMT markers, extracellular matrix, and associated signalling pathways by long non-coding RNAs in glioblastoma mesenchymal transition: A scoping review. Biology (Basel) 12: 818, 2023.
37. Joseph JV, Conroy S, Tomar T, Eggens-Meijer E, Bhat K, Copray S, Walenkamp AM, Boddeke E, Balasubramanyian V, Wagemakers M, *et al*: TGF-β is an inducer of ZEB1-dependent mesenchymal transdifferentiation in glioblastoma that is associated with tumor invasion. Cell Death Dis 5: e1443, 2014.
38. Chen J, Hu J, Li X, Zong S, Zhang G, Guo Z and Jing Z: Enhydrin suppresses the malignant phenotype of GBM via Jun/Smad7/TGF-β1 signaling pathway. Biochem Pharmacol 226: 116380, 2024.
39. Corbet C, Bastien E, Santiago de Jesus JP, Dierge E, Martherus R, Vander Linden C, Doix B, Degavre C, Guilbaud C, Petit L, *et al*: TGFβ2-induced formation of lipid droplets supports acidosis-driven EMT and the metastatic spreading of cancer cells. Nat Commun 11: 454, 2020.
40. Song C and Zhou C: HOXA10 mediates epithelial-mesenchymal transition to promote gastric cancer metastasis partly via modulation of TGFB2/Smad/METTL3 signaling axis. J Exp Clin Cancer Res 40: 62, 2021.
41. Almstedt E, Rosén E, Gloger M, Stockgard R, Hekmati N, Koltowska K, Krona C and Nelander S: Real-time evaluation of glioblastoma growth in patient-specific zebrafish xenografts. Neuro Oncol 24: 726-738, 2022.
42. Larsson S, Kettunen P and Carén H: Orthotopic transplantation of human paediatric high-grade glioma in zebrafish larvae. Brain Sci 12: 625, 2022.